5-1-2023

Experimental and numerical investigation of the effect of water cooling on the temperature distribution of photovoltaic modules using copper pipes

Mohammad Hassan Shojaeefard

Noor Barzan Sakran

Mohammad Mazidi Sharfabadi

Omar A. Hussein

Hussein A. Mohammed
Edith Cowan University

Experimental and Numerical Investigation of the Effect of Water Cooling on the Temperature Distribution of Photovoltaic Modules Using Copper Pipes

Mohammad Hassan Shojaeefard [1,*](ID), **Noor Barzan Sakran** [1,2], **Mohammad Mazidi Sharfabadi** [3], **Omar A. Hussein** [4] **and Hussein A. Mohammed** [5,*](ID)

1 School of Mechanical Engineering, Iran University of Science and Technology (IUST), Tehran 13114-16846, Iran
2 Presidency of Ministers, Foundation of Martyrs, Nassiriya 64001, Thi-Qar, Iraq
3 Developments and Optimization of Energy Technologies Division, Research Institute of Petroleum Industry (RIPI), Tehran 14856-13111, Iran
4 Petroleum System Control Engineering Department, College of Petroleum Processes Engineering, Tikrit University, Tikrit 34001, Iraq
5 School of Engineering, Edith Cowan University, 270 Joondalup Drive, Joondalup, WA 6027, Australia
* Correspondence: hussein.mohammed@ecu.edu.au (M.H.S.); mhshf@iust.ac.ir (H.A.M.)

Abstract: In hot climates, PV efficiency drops dramatically if the surface temperature of the panels rises over a specific limit. Consequently, a cooling system is required to preserve PV modules as close to their operating temperature as feasible. For this purpose, the influence of an increase in PV surface temperature on PV performance was studied experimentally and numerically at the Research Institute of Petroleum Industry (RIPI) in July. The current study uses a cooling system consisting of rows of copper pipes connected to the PV backside. The experiments are conducted for four distinct scenarios, each with a different input fluid temperature ranging from 19.5 to 61 °C. The parametric analysis focuses on three influential factors: ambient temperature, solar radiation, and fluid inlet temperatures. In addition, other inputs are configured in accordance with the experimental conditions. The results showed that installing a cooling water system decreased the PV surface temperature from 60.20 °C to 40.24 °C at 9:00 am and from 73.98 °C to 73.33 °C at 1:30 pm. Furthermore, the electrical, thermal, overall, and exergy efficiencies drop as radiation intensity and water inlet temperature increase. In addition, the numerical results are validated with the experimental ones, and it shows high degrees of concordance.

Keywords: solar thermal; thermal–photovoltaic hybrid collector; thermal modeling; electrical and thermal efficiency; solar thermoelectric cooler

1. Introduction

The previous several years have seen a rise in interest in alternative forms of energy, including solar energy [1,2]. Solar energy has several uses, including solar cell power production, solar thermal utilization, and photochemical conversion. In the field of renewable energy, photovoltaics (PV) stands out as a promising technology [3]. However, increasing solar cell efficiency is one of the most hotly debated issues in the PV industry. In order to maximize the PV module's efficiency, the operating temperature of its surface must be kept to a minimum. Therefore, it is vital to cool the photovoltaic module in order to disperse the heat from the photovoltaic cells [4,5]. Thus, much research has focused on various cooling strategies for PV cells [6,7]. According to [8–10], the most practical techniques are impinging jets and channels since they have sufficiently low thermal resistance to provide adequate cooling performance. Furthermore, heat transfer improvement is made possible by the capacity of the channel pipe heat sink to absorb a significant quantity of heat from a

tiny area. Consequently, academics have focused on developing cooling technologies by channel pipe heat sinks for various applications [11–13].

In recent years, experimental and numerical studies on the effect of various cooling pipe forms on the performance of solar cells have increased.

According to Siddiqui et al. [14], cooling solar modules enhanced electrical output from roughly 80 W to 120 W at 1000 W/m^2 in contrast to uncooled panels. In addition, Teo et al. [15] found that using the cooled panels led to an approximately 45% improvement in the solar cells' efficiency. In a different piece of research, Bahaidarah et al. [16] discovered that the energy output of their photovoltaic system was 190 watts when it was not cooled, but it increased to 750 watts when water cooling was applied to the same panels. Bashir et al. [17] researched to determine the impact of water-based solar cell cooling. Both monocrystalline and polycrystalline photovoltaic cells were utilized in this project. They observed that the performance of photovoltaic panels has increased. Shuang-Ying et al. [18] developed a theoretical model to investigate the heat transfer properties and efficiency of a cooling channel installed on the solar cell's top surface. As a direct result, PV/T has substantially higher thermal efficiency compared to a traditional system. Chaoqun et al. [19] designed several distinct parallel cooling channels to investigate the influence of these channels on the PV/T collector efficiency. According to the findings, the temperature of the solar modules is lowering and becoming more equally distributed. The finite element approach was used by Afroza Nahar et al. [20] in order to carry out a three-dimensional numerical study of the PV/T system. The experiment was conducted outside under typical meteorological conditions. The outcomes demonstrated that the maximum total PV/T system efficiency was determined to be 84.4% numerically and 80% experimentally under 1000 W/m^2 of irradiance conditions and inlet and ambient temperatures of 34 °C. Chao Shen et al. [21] have developed a PV/T system based on field synergy theory that uses a specific cooling channel to maximize the PV/T system's efficiency. Mathematical models for the novel PV/T system were confirmed using experimental data, and their performance was examined numerically. When the cooling water intake flow rate rose from 0.0018 kg/s to 0.018 kg/s, the electrical efficiency rose from 10.8% to 11.9%. In hot climates, PV/T system numerical simulations are carried out by Tareq Salameh et al. [22]. Eleven channels are placed in a row on the PV bottom module for cooling purposes. Comparing a PV with a cooling system to one without cooling, the cooling system enhanced thermal efficiency.

The accumulation of dust on the surface of solar panels can have a significant impact on their efficiency and performance. When dust accumulates on the surface of a solar panel, it restricts the sun's rays from reaching the solar cells, which reduces the amount of energy that can be generated [23,24]. In this study, negligible dust effects were assumed.

According to H. Demir et al. [25], they conducted research that involved collecting and transferring thermal energy from a PV panel to a thermoelectric generator (TEG). They created a temperature gradient by decreasing the temperature through the use of an aluminum heat sink in typical weather conditions. The generated temperature gradient was then utilized to produce electricity using two TEGs. The researchers measured the highest temperature gradient resulting from solar radiation to be 21.08 °C.

Bhakre et al. [26] reported that the conversion efficiency of a typical PV system is between 15% and 20%, which means that only a fraction of the solar energy that strikes the panel is converted into electricity. The remaining energy is converted into heat, which raises the temperature of the PV cell. If the temperature of the PV cell exceeds the recommended operating temperature, the efficiency of the PV system decreases, which leads to a decrease in power output. Therefore, it is important to design PV systems to minimize the temperature increase in the PV cells, such as by incorporating cooling systems or using materials with high thermal conductivity.

Many researchers have reviewed the effect of different cooling types, such as active cooling (using water and air medium) and passive cooling (heat pipe and wick structures, phase change materials). They also discuss the different designs of solar thermal absorber collectors, technical aspects, cooling methods, and development in the cooling system

of PV panels. The use of PCMs, nanofluids, and different flow configurations shows improvements in the performance of the PV/T system [27,28].

Bhandari et al. [29], seven different configurations were numerically evaluated to determine the heat sink with the best thermo-hydraulic performance using water as the working fluid and copper as the substrate material. The variations in side ranged from 3 to 9, ANSYS Fluent 18.0—The commercial code ANSYS Fluent V18.0 software was used to simulate several heat sink models. In addition, the parameter prism radius was also examined for the best-performing heat sink configurations.

In summary, for PV/T collector thermal management and reliability, using cooling channels is an effective means of achieving excellent thermal efficiency for the PV/T collector. The influence of cooling channels on PV/T collector thermal performance has also been studied extensively, and various attempts have been made to improve cooling channel heat transfer. The primary concerns in these earlier investigations were the photovoltaic modules' decreased average temperature and more excellent thermal uniformity. However, for PV/T collectors with parallel cooling pipes, the fundamental mechanism for how the structural parameter of parallel cooling pipes affects heat transfer is still unclear.

This paper uses experimental and numerical analysis to compare the efficiency of a traditional PV module and a hybrid PV/T module with a cooling water system in hot climatic in Iran. To maximize both electrical power production and thermal energy, the rear of the PV panel is cooled using a row of copper pipes, with the water temperature being varied as input.

The main goals of the current study are:

1- Study some parameters that affect the performance of the PVT system experimentally (with and without cooling) in Tehran, Iran, in hot weather depending on the actual hourly data such as solar radiation, ambient temperature, and inlet water temperature;
2- To disseminate the culture of depending on renewable energy systems in Iran to reduce dependence on national electricity in the future.

2. The Study Methodology

Overview of the Novel Configuration of PVT

The primary parts of a PVT system are the heat collector and the PV panel. The collector comprises the following components: a single-glass cover with an area of 1.48 m^2 and a photovoltaic module capable of producing up to 250 watts of electricity. The photovoltaic module has sixty sun cells that are made from monocrystalline silicon. The module's dimensions are 165 cm $\times$ 156 cm, and each solar cell has an area of 0.0243 m^2. As can be seen in Figure 1, the absorber collector was fabricated out of copper pipes. The heat loss from the sides and bottom of the absorber collector was reduced by securing the thermal insulator there. The copper water pipes were linked to the bottom of the aluminum plate that made up the absorber. The MHP generates energy from the c-Si solar cells and delivers that heat to the flowing inlet water. Studying the effects of flow arrangement and design on thermal performance and temperature dispersion in PVT collectors was the primary motivation for this investigation.
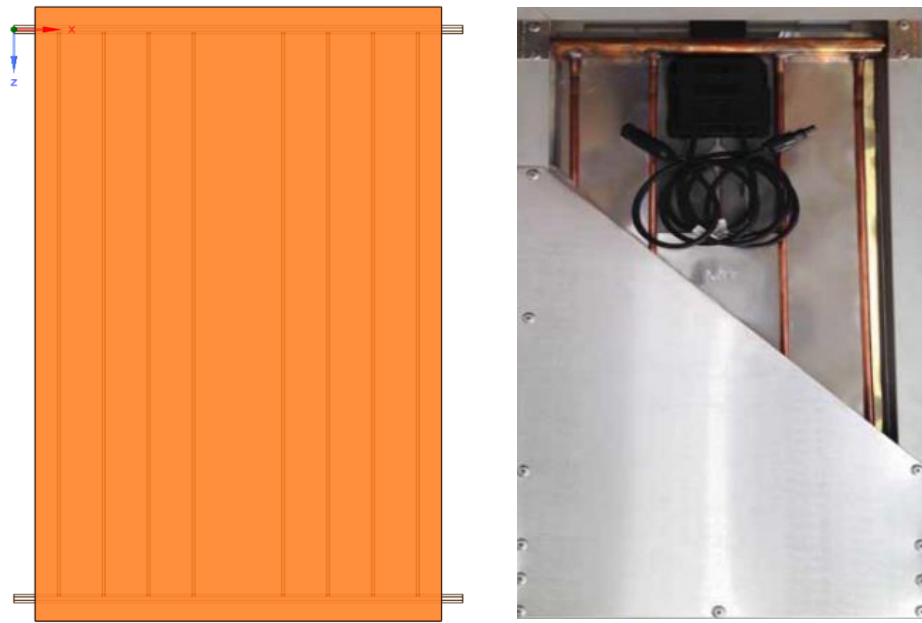
Figure 1. Monocrystalline panel module.

3. Experimental Setup

In this investigation, a hybrid photovoltaic (PVT) solar system is used, which has been set up on the roof of the Research Institute of the Petroleum Industry (RIPI) in Tehran, Iran. This structure is located at a latitude of $36°51'41.0''$ N and a longitude of $51°15'32''$ E, both of which contribute to the local climate. Experiments were carried out under steady-state circumstances to measure the PVT absorber's thermal and electrical output.

The short-circuit current (I_{sc}), open-circuit voltage (V_{oc}), voltage and current at maximum power point (MPP), load voltage curve, useful energy (Q), and total efficiency (η) were all measured alongside the global irradiance (G), inlet water temperature (T_{in}), ambient temperature (T_{amb}), outlet water temperature (T_o) and wind speed (V) in this experiment. The experimental test rig includes a storage water tank with a capacity of (200 L), a pump, a flow meter with a flow regulator, a chiller, an air cooler, an electric heater, an auxiliary heater, a PV panel, a PVT system, heat sensor, heat exchanger, and data acquisition apparatus. In addition, the model data logger (Adam) was also connected to the PC. The collector's intake and exit pipe walls are equipped with temperature sensors. Solar radiation has been measured using a pyrometer with a (0–2000) W/m^2 range and a precision of 0.1%.

Furthermore, the wind velocity has been calculated using an IEC61400-12 anemometer with an accuracy of ±0.5 m/s. Finally, the voltage, current, and resistance are measured using the electrical heater in short-circuit conditions. The digital multimeter has been employed for this purpose. Measurement data from many instruments were collected in real time with the program's help.

The PVT water system test rig and schematic, seen in Figure 2, consists of a PVT water collector, heat exchanger, storage tank, air cooler, chiller, flow meter, temperature sensor, filter, and water pump. First, the inlet pipe was connected to a tank with cold water to fill the cooling system with water. After that, the tank valve closes, and the cooling water cycle becomes closed. Then, the mass flow rate is measured and passed through two temperature sensors (primary and secondary). In the first practical experiment, the outlet water of the cooling system is not cooled but is pumped back into the inlet pipe. In other words, cooling systems such as air coolers, heat exchangers, and chillers are not utilized to chill the water that flows out of the PV system's cooling pipes. Therefore, the inflow water is heated as it circulates through the collector's pipes. In order to gather the required data, the system uses several different measurement devices. A spreadsheet was developed to analyze the

experiment's findings and keep track of the daily measurements taken throughout the experiment. The specification and materials properties of the PV are given in detail in Tables 1 and 2.

(a)

(b)

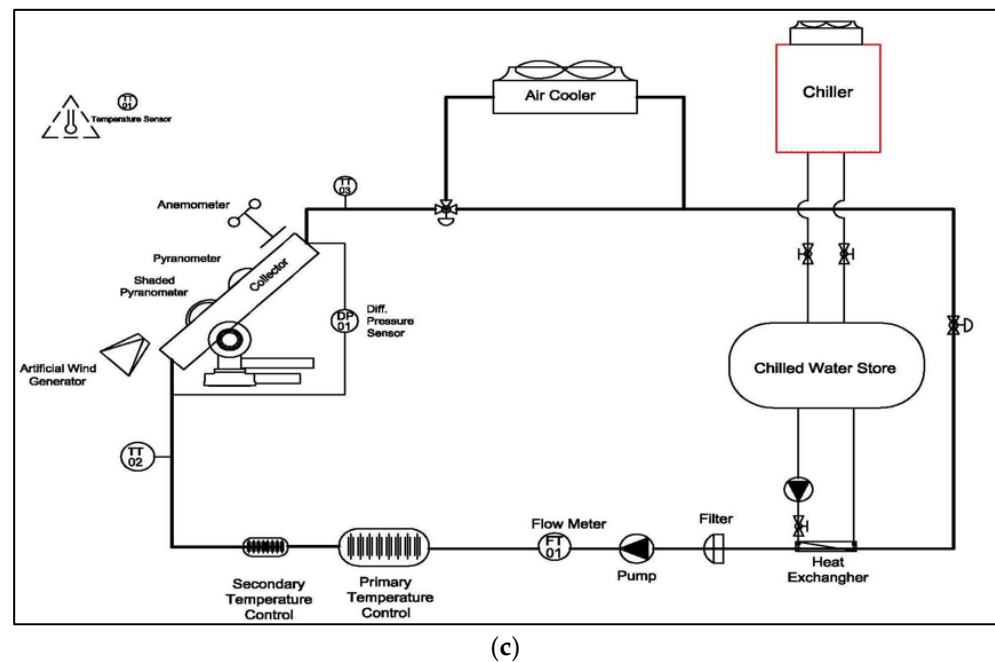**Figure 2.** *Cont.*

(c)
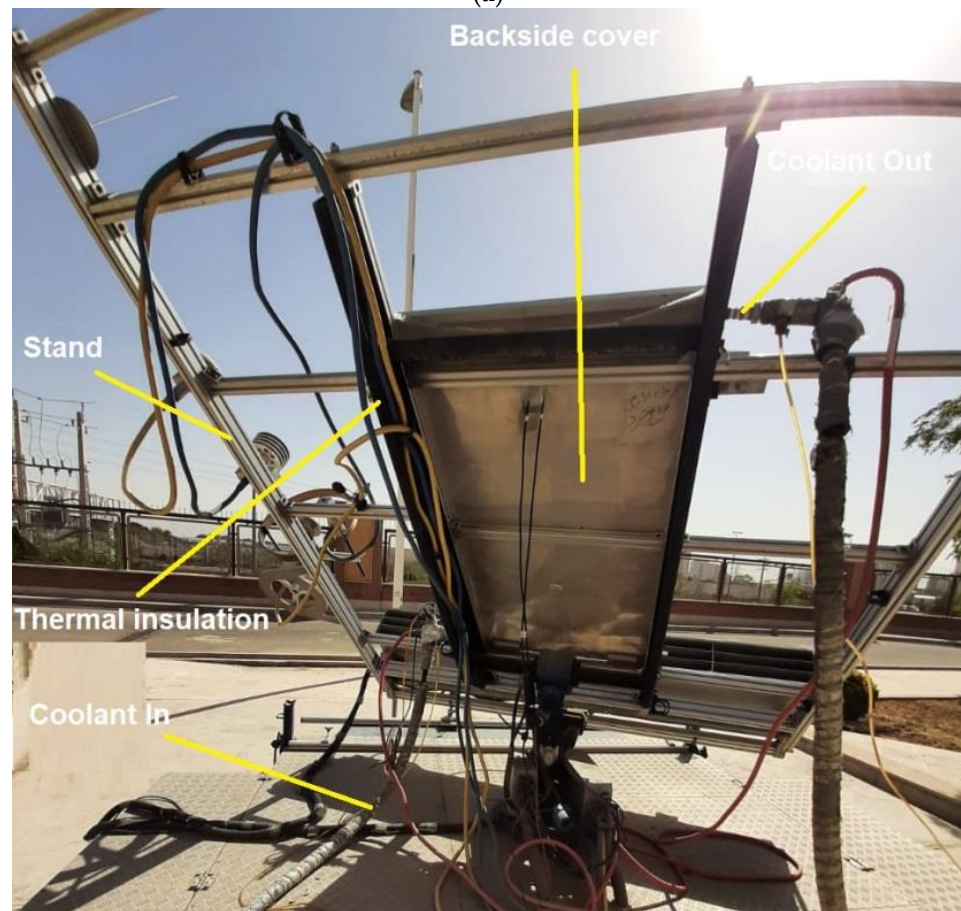
Figure 2. (**a**): System with measurement devices, (**b**): back views with main, and (**c**): schematic diagram of a PVT system.

Table 1. Specification of materials properties of the PV.

Layers	k (W/mk)	Cp (J/kg, K)	ρ (kg/m^3)
Glass	2	500	2450
EVA	0.311	2090	950
Polycrystalline cell	148	700	2329
Tedlar	0.15	1250	1200

Table 2. Specifications of the PV system.

Measuring Device	Measuring Range	Precision	Total Response
Thermometer	$-40 + 60\ ^\circ$C	± 0.01	<10 s
Pyranometer	0–2000 W/m^2	$\pm\%0.2$	20 s
Anemometer (air velocity)	0–50 m/s	± 0.01 m/s	<10 s

3.1. Uncertainty Analysis

The inaccuracies present in measuring devices can impact the SPV-THC's ability to make accurate predictions regarding thermodynamic performance. To estimate the potential errors in calculated thermodynamic performance metrics, the typical approach involves using the following equation [30]:

$$e_{\text{R}} = \left[\left(\frac{\partial R}{\partial V1} e_1 \right)^2 + \left(\frac{\partial R}{\partial V2} e_2 \right)^2 + ... + \left(\frac{\partial R}{\partial Vn} e_n \right)^2 \right]^{0.5} \tag{1}$$

The equation used to determine the uncertainty of function *R* involves the independent variables V_1, V_2, ... V_n and the uncertainty value e_{R}. The electrical, thermal, and overall efficiency uncertainties were measured to be approximately $\pm 5.2\%$, $\pm 2.4\%$, and $\pm 3.89\%$, respectively. More details regarding the instrument specifications are provided in Table 3.

Table 3. Technical details of instruments.

Device	Operating	Accuracy
Flow meter	0–90 L/h	±3%
Data logger	0–1200 °C	±0.8%
Temperature	0–200 °C	±0.2 °C
Thermometer	0–150 °C	±0.15
Pyranometer	0–1900 W/m^2	±5 W/m^2
Relative humidity	0–100%	±2%
Anemometer	0–20 m/s	±0.01 m/s
Fluid pressure drop	0–25 kPa	±0.3%
Amps	0–40 Amps	±0.5 Amps
Volts	0–440	±5 V
Photovoltaic power output	0–2000 W	±3 W

3.2. Data Reduction

Convective heat transfer q_{cg}, in which heat is lost from within to outside through the glass cover, can be represented mathematically as

$$q_{cg} = h\left(T_g - T_{amb}\right) \tag{2}$$

T_{amb} and T_g are the ambient and glass temperatures, respectively, and the external heat transfer coefficient (W/m^2 K) is h, which can be obtained from [31].

$$h = 5.7 + 3.8V_{wind} \tag{3}$$

Radiant heat losses between the outside environment and the glass results in heat loss, represented by q_{rg}, which may be written as

$$q_{rg} = \varepsilon_g C_0 \left[\left(\frac{T_g}{100}\right)^4 - \left(\frac{T_{sky}}{100}\right)^4 \right] \tag{4}$$

The glass emissivity is represented by ε_{g1} = 0.94; the blackbody's radiation coefficient is C_0 = 5.67 W/(m^2 K^4); the sky temperature is T_{sky}, which can be calculated by [32] as flowing:

$$T_{sky} = 0.0552 T_{amb}^{1.5} \tag{5}$$

The $q_{pv,\alpha}$ is the PV panel's solar energy absorption, which is determined by

$$q_{pv,\alpha} = p\tau_g \alpha_{pv} G(t) \tag{6}$$

Solar electric energy (q_e) created by the PV can be written as

$$q_e = \eta_e \tau_g \alpha_{pv} G(t) \tag{7}$$

The cell packing factor is indicated by p.; η_e represented the PV efficiency against the temperature [13]

$$\eta_e = \eta_c \left[1 - 0.0045\left(T_{pv,ave} - 298.15\right)\right] \tag{8}$$

where $T_{pv,ave}$ represents the whole PV total average temperature, and under standard conditions, η_c represents the nominal electrical efficiency.

The electrical efficiency of the PV module can be described by the following equation:

$$\eta_e = \frac{V.I}{A_c G(t)}$$

Calculating the radiative heat transfer (q_{rpv}) and the convective heat transfer (q_{cpv}) between the outside environment and PV panel as follows:

$$q_{rpv} = \varepsilon_{g2} C_0 \left[\left(\frac{T_{pv}}{100} \right)^4 - \left(\frac{T_{sky}}{100} \right)^4 \right] \tag{9}$$

$$q_{cpv} = h(T_{pv} - T_{amb}) \tag{10}$$

The emissivity of the glass is $\varepsilon_{g2} = 0.94$ and T_{pv} is the temperature of the PV.

The equation for the practical heat exchange between the PV panel and the fluid of the cooling pipe is

$$q_{pv} = q_{pv,\alpha} - q_{cpv} - q_{rpv} - q_e \tag{11}$$

Most studies focused on the first efficiency law to assess the efficiency of air-cooled PV/T systems.

A water-cooled PVT thermal efficiency is defined by [33] and written as:

$$\eta_{th} = \frac{m c_p (T_{out} - T_{in})}{A_c I} \tag{12}$$

To obtain the total energy efficiency of the cooled PVT system, the formula is as follows:

$$\eta_{total} = \eta_{th} + \eta_{e,ave} \tag{13}$$

After having determined the absorber plate mean temperature, T_{ap}, the bottom heat loss coefficient U_b, representing the conduction heat loss away from the absorber plate to the environs, can be expressed using Fourier's law as:

$$Q_b = k_{ins(b)} A_C \frac{(T_{ap} - T_a)}{thk_{ins(b)}} = U_b A_C (T_{ap} - T_a)$$

$$U_b = \frac{k_{ins(b)}}{thk_{ins(b)}} = \frac{Thermal\ conductivity\ of\ insulation\ at\ bottom}{Thickness\ of\ insulation\ at\ bottom}$$

Similarly, the edge heat loss U_e, from the FPSC to the surrounding is:

$$Q_e = k_{ins(e)} A_e \frac{(T_{ap} - T_a)}{thk_{ins(e)}}$$

Since all heat loss coefficients are referenced to the same area as denoted the collector area, A_c; hence, Equation (14) was reformed as:

$$Q_e = \frac{k_{ins(e)} A_e}{A_C} A_C \frac{(T_{ap} - T_a)}{thk_{ins(e)}} = U_e A_C (T_{ap} - T_a) \tag{14}$$

$$U_e = \frac{k_{ins(e)} A_e}{thk_{ins(e)} A_C}$$
$$= \frac{Thermal\ conductivity\ of\ insulation\ at\ edge \times Edge\ Area}{Thickness\ of\ insulation\ at\ bottom \times Collector\ Area} \tag{15}$$

The total exergy efficiency of PVT is obtained by [34].

$$\eta_{ex} = \frac{Ex_{pv} + Ex_{th}}{Ex_{sun}} \tag{16}$$

$$Ex_{sun} = \left[1 + \frac{1}{3} \left(\frac{T_{amb}}{T_s} \right)^4 - \frac{4 T_{amb}}{3 T_s} \right] I(t) A_c \tag{17}$$

$$Ex_{pv} = \eta_{e,ave} I(t) A_c \tag{18}$$

$$Ex_{th} = mc_p(T_{out} - T_{in})\left(1 - \frac{T_{amb}}{T_{out}}\right) \tag{19}$$

PV solar cells' total electrical exergy is represented by Ex_{pv}, the output of overall thermal exergy is Ex_{th} and the input exergy of solar radiation is Ex_{sun}. The sun's temperature, T_s, is 5760 K [34].

4. Mathematical Modeling

The experimental geometry gathered from the (instituted) was used to guide the selection of a benchmark model. Aluminum absorber plates with a thickness of 1 mm, copper pipes running parallel to the absorber plates, and glass measuring 0.03 m were the distinguishing features of the PV. There is a spacing of 0.1125 m between riser pipes, and the pipes were joined to the absorber plate. According to Figure 3, the tube risers are linked to two main headers at the inlet and the system's output.
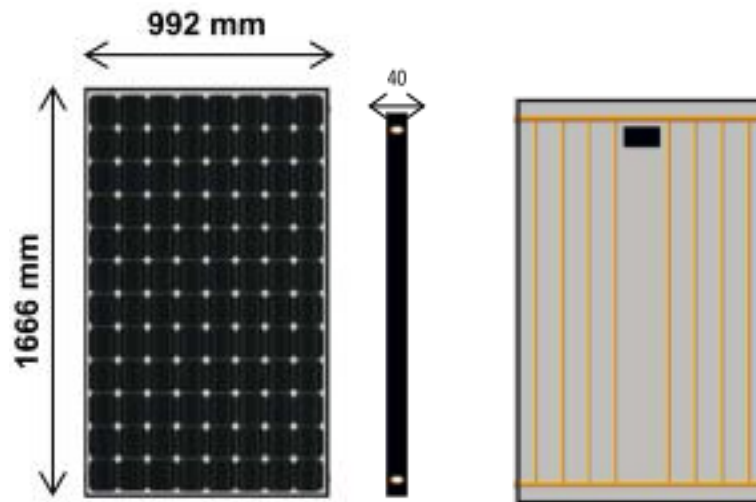

Figure 3. PV model.

4.1. Governing Equations

Inside the collector, the incompressible water fluid is governed by continuity, momentum, and energy equations. The appropriate expressions for these equations are as follows:
Continuity equation:

$$\nabla . \vec{V} = 0 \tag{20}$$

Momentum equation:

$$\frac{\partial \vec{V}}{\partial t} + \left(\vec{V}.\nabla\right)\vec{V} = -\frac{1}{\rho}\nabla p + v\nabla^2\vec{V} + \rho\vec{f} \tag{21}$$

energy equations

$$\rho C_p\left[\frac{\partial T}{\partial t} + \left(\vec{V}.\nabla\right)T\right] = k\nabla^2 T + \varphi \tag{22}$$

The continuity, momentum, and energy equations were numerically solved using a three-dimensional CFD model to estimate the temperature distribution in the PV panel and the water flow. The program ANSYS (22 r1) was used to do this. An adequate mesh network was constructed for the models using ANSYS meshing technology. To ensure the independence of the grid-based findings, an independence test was performed.

The simulation was performed with a convergence criterion of 10^6. Table 4 displays the climatological and physicochemical characteristics of the various strata and constituents.

Table 4. The basic components of the solar cell module with its properties. Reprinted with permission from Ref. [35].

Layer	Specific Heat, Cp. (J/kg, K)	Density, ρ. (kg/m^3)	Thermal Conductivity, k. (W/m.K)
Glass	500	3000	1.8
EVA	2090	950	0.312
PV cells	700	2330	149
Tedlar	1250	1200	0.2
Aluminum plate	887	2700	206
Copper pipe	381	8978	387.7
Cooling water	4182	998.2	0.6

4.2. Grid Independence

In order to produce reliable computational results unaffected by the grid's number or the cell size in the computational domain, CFD simulations must undertake grid independence research. This is necessary so that correct results can be achieved from simulations. This trend created coarse, medium, and fine meshes in succession. ANSYS's fluid meshing tool was used to produce the mesh. The computational domain's glass, photovoltaic cells (PV), absorber plate, pipes, and water were studied for grid independence.

In the grid independent test (GIT), test glass average temperature was tested numerically, as shown in Figure 4. Table 5 reveals that the second to third simulation state error ratio is 0.7%, which does not substantially alter simulation outcomes. Results for elements 6,418,042 and 6,815,325 were almost identical regarding the plate temperature. Therefore, the size of the mesh 6,418,042 was used for the simulation to decrease the processing time required.
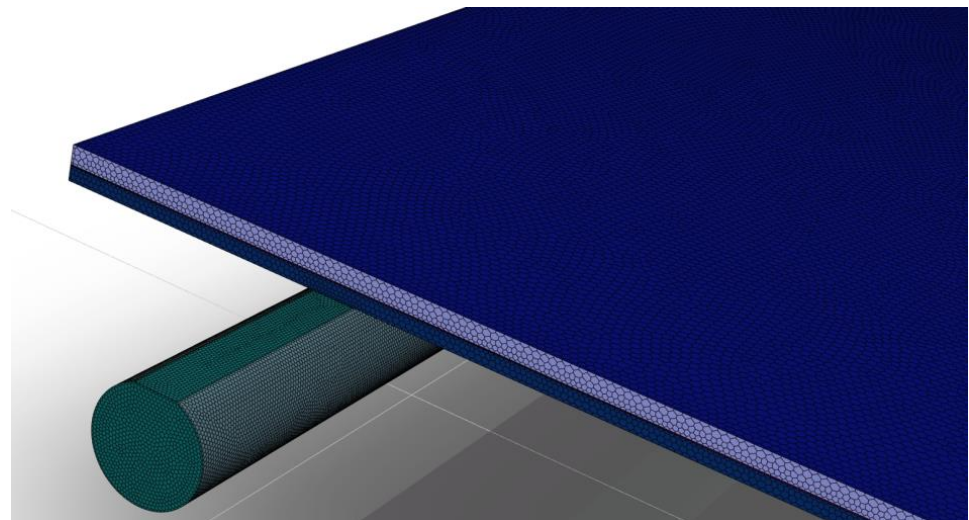

Figure 4. Grid layout of numerical simulation.

Table 5. Grid independent study for the PV computational domain.

Number of Element	Average Temperature (°C)	Error %
5,565,242	60.35	—
6,418,042	66.6	10.35%
6,815,325	67.1	0.7%

5. Results and Discussions

Convective heat flow via solar panels has been conducted experimentally and numerically in this section, and the findings are shown. For a solar panel to be efficient, the backside temperature must be kept as low as feasible. Research on the heat transfer of solar panels' backsides has shown that a rise of 1 K in surface temperature causes a 0.5% decrease in the PV module's efficiency. This demonstrates the criticality of this area of research. Therefore, the solar panel's temperature is studied in this research to find the impacts of heat flux on the panel's parameters. In addition, solar panels may receive varying levels of solar energy throughout the day. Therefore, varying heat flux values were used in this investigation to simulate the impact of different solar radiation rates.

The experiments are conducted in four stages at different fluid inlet temperatures, whereby the fluid inlet temperature is incrementally raised from 19 °C to about 61 °C. The collected data include fluid inlet and exit temperatures, mass flow rate, wind velocity, and solar radiation. In Table 6, these facts are presented delicately.

Table 6. Ambient and PVT conditions of experimental tests.

Case No.	Step No.	I (W/m^2)	Ta (°C)	Tin (°C)	U (m/s)	m (kg/s)
1	1	963	17.3	20	3	0.033
	2	969	17.6	20	2.8	0.033
	3	990	17.7	20	2.7	0.032
	4	979	18.1	19.2	2.3	0.033
2	1	1018	18.7	33.3	2.5	0.032
	2	1014	18.5	33.8	3.1	0.033
	3	1010	18.6	33.4	2.7	0.033
	4	1002	18.9	33.9	2.8	0.032
3	1	1008	19	46.7	2.6	0.032
	2	1032	19.1	47.4	2.9	0.032
	3	1018	19	46.5	2.8	0.032
	4	974	18.8	46.4	3.5	0.032
4	1	982	19.9	61.3	2.5	0.032
	2	981	20.1	61.1	2.7	0.032
	3	980	19.8	61.5	2.8	0.032
	4	989	20.1	61.7	2.8	0.032

5.1. Model Validation

The operating parameters, which comprised the ambient temperature, solar radiation, and fluid intake temperature for the PVT, were established according to the experimental work. The CFD model was tested assuming that the wind speed was 3 m/s. The meteorological data (solar radiation and ambient temperature) and inflow water temperature were recorded throughout the day of the experiment and are shown in Figure 5. These data served for use as the validation's input conditions carried out in the present research.

An hour-and-a-half interval was regarded as an input parameter to verify the CFD model used to represent the PV. These actions were taken under the parameters in Figure 3. An hourly and a half-interval report of the simulation results was calculated separately (outlet temperature) for the pipe, and the experimental findings were compared to those from numerical simulations. The pattern observed in the experiment was followed by the output water temperature in this investigation, as shown in Figure 6, with a relative error of 1%. This validation demonstrates that this model accurately predicts the temperature at the outflow compared to the data gathered from the experiments. However, there are discrepancies between the experimental data and the numerical results. This might be because the simulation uses input insolation data based on fitting the actual data to a polynomial curve at the fourth order, which does not adequately depict the unpredictable swings in actual insolation values, as seen in experimental measurement.
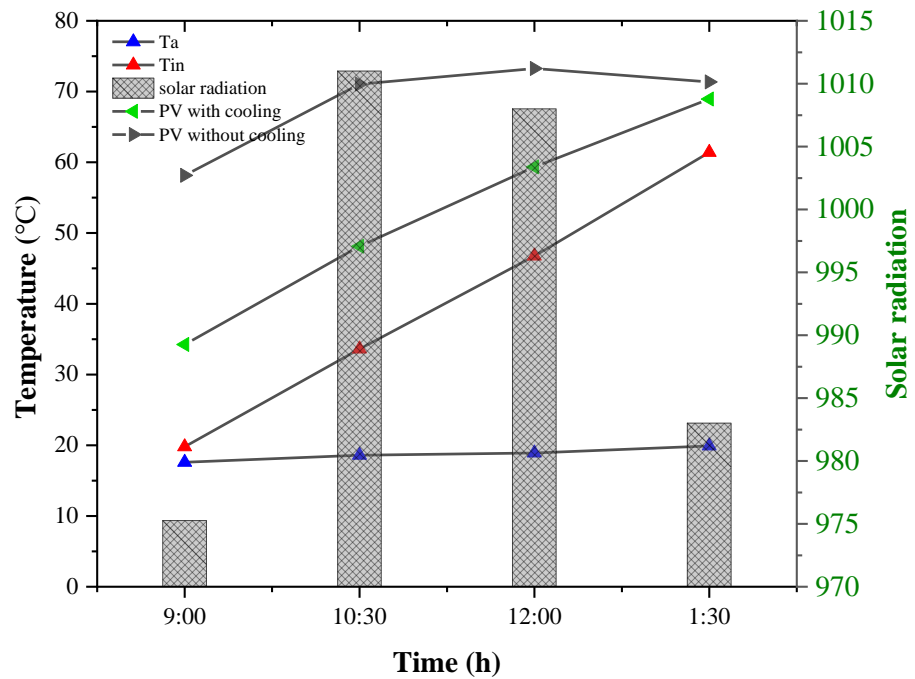
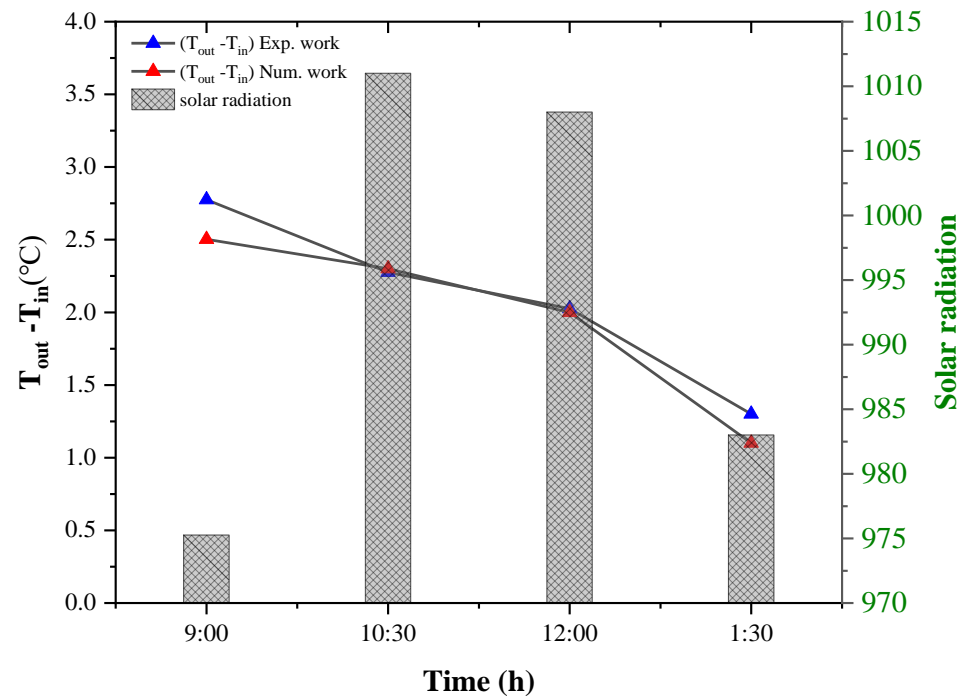**Figure 5.** Experiments ambient temperature, solar radiation, and water temperature at the inlet.

Figure 6. Experiment and numerical comparison of outlet fluid temperature.

5.1.1. Solar's Average Temperature

Figure 5 shows experimentally and numerically the hourly PV surface temperature that records for both reference (PVR) without cooling and cooling water (PVT) for several inlet water temperatures. The water temperature entering the system ranges from 19.5 °C. to 61 °C. The ambient airflow was maintained at 3 m/s, and the temperature was held at 20 °C for both the PVR and the PVT. Experimentally, the surface temperatures of the PV cells are recorded hourly and a half at six evenly spaced locations throughout each of the PV modules under study. Average surface temperatures for the PVR and PVT under varying

amounts of solar radiation are shown in Figure 7. The PVR module surface temperature was determined to be 58, 71, 73, and 71.5 °C. In contrast, the PVT module temperature rises linearly with water cooling and ranges from 33 to 69 °C for induced water input temperatures between 19.5 and 61 °C. The highest value for the PV surface temperature of cooling modules was obtained at 1:30 pm, whereas the maximum value for the reference model without cooling was attained at 12:00 noon. It is noted that when sun radiation rises, so does the temperature of the cooling PVT. Due to an increase in solar radiation, the incoming water will be warmer. To further clarify, with increasing radiation intensity, the outlet temperature of the water will increase since it will be pumped back into the water inlet pipe; the PV temperature will rise due to the higher incoming water temperature. The PVR temperature was around 29 °C greater than the module PVT temperature in the morning and 3 °C at the closure of test day. It is noted that the difference between PVT and PVR temperature is close at the end of the examination. This is because the inlet water temperature is high and almost reaches the temperature of PVR, so the cooling efficiency is practically absent. It can be shown that the experimental curve closely matches the numerical pattern, with some minor discrepancies attributable to experimental control parameters and sensor errors.
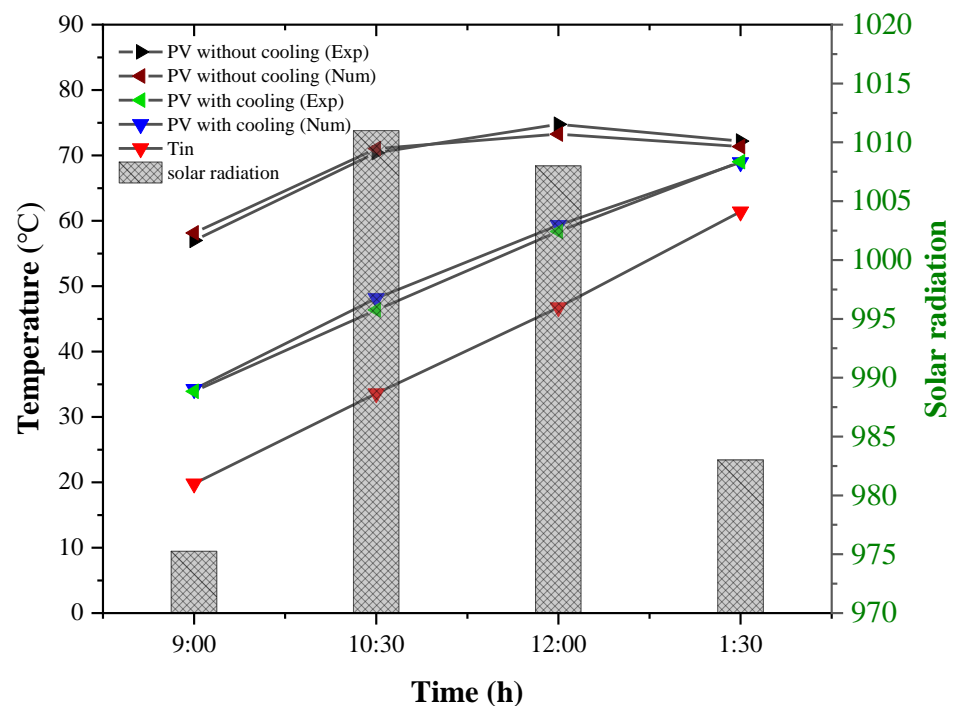

Figure 7. Experimentally and numerically, the hourly PV surface temperature with different solar radiation.

5.1.2. Analyze Simulation Models

The PV temperature contours with and without cooling for the four stages are shown in Figure 8 to evaluate the temperature scattering in the current numerical simulation. The numerical simulation depicts the temperature distribution with collector fluid entering the panel at a flow rate of 0.033 kg/s, a temperature of 19.5 to 61 °C, and varying solar radiation over the day. In addition, the model's design reveals that the absorber plate's backside is connected to the tubes. Therefore, the effect of the cold fluid in the pipes on the PV and fluid temperature can be easily detected by evaluating the temperature contours and simulation outcomes.
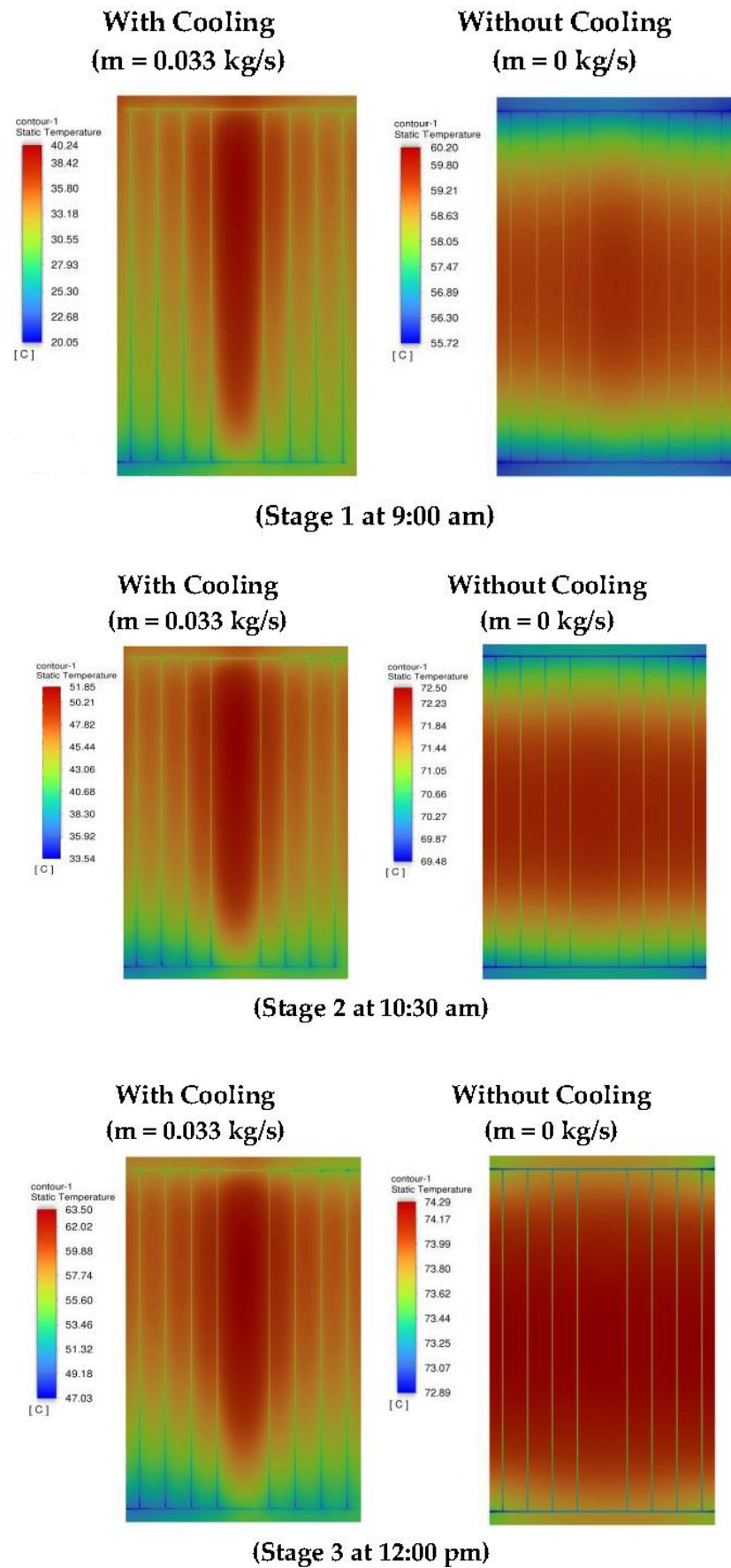
(Stage 1 at 9:00 am)

(Stage 2 at 10:30 am)

(Stage 3 at 12:00 pm)
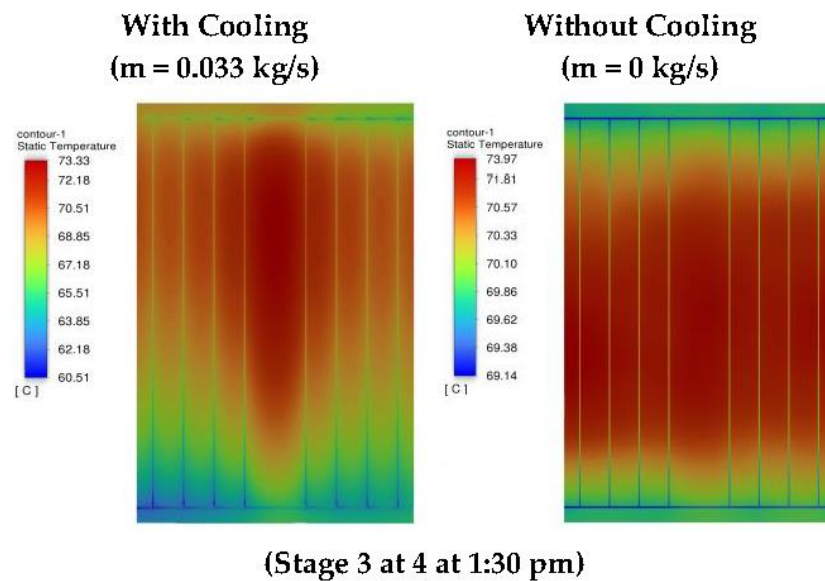
Figure 8. *Cont.*

Figure 8. PV temperature distribution at the four stages.

For the solar cell in Figure 8, stage 1, it is clearly seen that the surface temperature of the cell at the water inlet is cooler than that at the water outlet. The reason for this is that the temperature of the inlet water is as low as possible. Then the temperature of the cell's surface gradually rises along the stages because the fluid inlet temperature is increased step by step, starting from 19.5 °C to approximately 61 °C during circulation through the collector's pipes, causing increasing the water temperature. Moreover, the temperature contour of the fourth stage shows that the temperature of the water at the outlet is almost equal to the temperature at the inlet, which causes the cell temperature to rise to the highest value at the highest solar radiation.

Furthermore, according to the PVT temperature contour, the center of the surface and the regions between the tubes has the greatest temperatures. This is because the tubes' cooling effects are not present in this area of the absorber plate. Therefore, temperatures are likely to rise since there is no efficient heat sink. In addition, the contour shows that the PV without cooling has the highest temperature than the PV with the cooling system. In addition, the temperature contour shows that the temperature at the center of the PV is the highest, and it increases with increasing solar radiation.

It seems that the statement discusses a study that investigates the importance of outlet coolant and PV temperatures in computing thermal and electrical efficiency in a PVT (photovoltaic thermal) system. The study compares the simulation results with daily experimental data and calculates the electrical and thermal efficiency of the PVT system based on both the experimental and simulated data.

Figure 9 presents the estimated results of the numerical simulations and the measured data of the experimental tests. The study claims that the simulation accurately estimates the daily experimental data, with a mean difference of less than 5% for both the outlet temperature of the nanofluid and the average PV temperature.

Overall, the study suggests that the numerical simulation method used in the experiment can effectively estimate the thermal and electrical efficiency of the PVT system and provide reliable results comparable to experimental data.
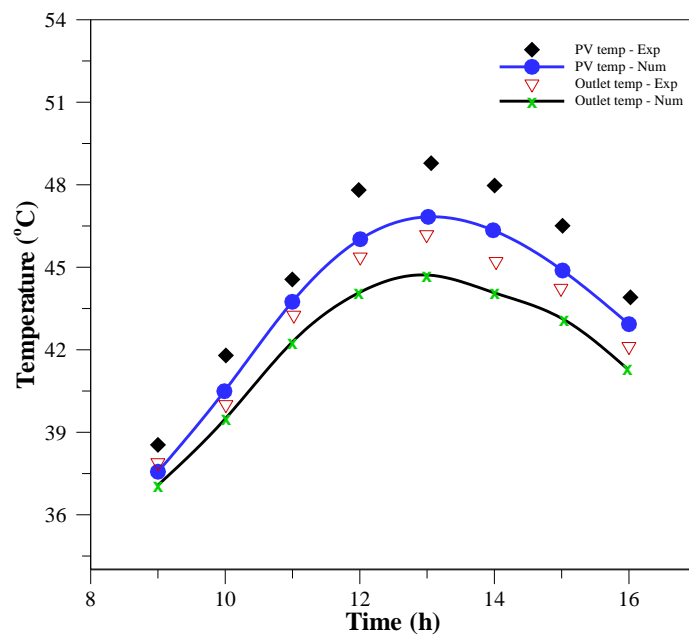
Figure 9. Numerical and experimental results of outlet temperature and PV mean temperature.

5.2. Electrical Efficiency

The incident solar radiation and electrical power production are used to determine the electrical efficiency. During July, Figure 10 displays the hourly variations in electrical efficiency for the PVR and PVT modules at a constant water mass flow rate of 0.033 kg/s and varying inlet water temperatures. The two modules' electrical efficiency is highest around 9.00 am. Further, the PVR and PVT modules' electrical efficiency significantly drops throughout the test period. In addition, Figure 7 shows that the PV module electrical efficiency is improved by 15% to 23% at 9.00 am, 9% to 18% at 12.30 pm, 8% to 16.5% at 2.30 pm, and 9% to 10% at 4.30 pm when a cooling water system is used. It has been observed that PVT's efficiency ultimately approaches that of PVR. As the inlet water temperature rises toward the PV temperature, the heat exchange rate between the water and the cell and decreases, causing this phenomenon.
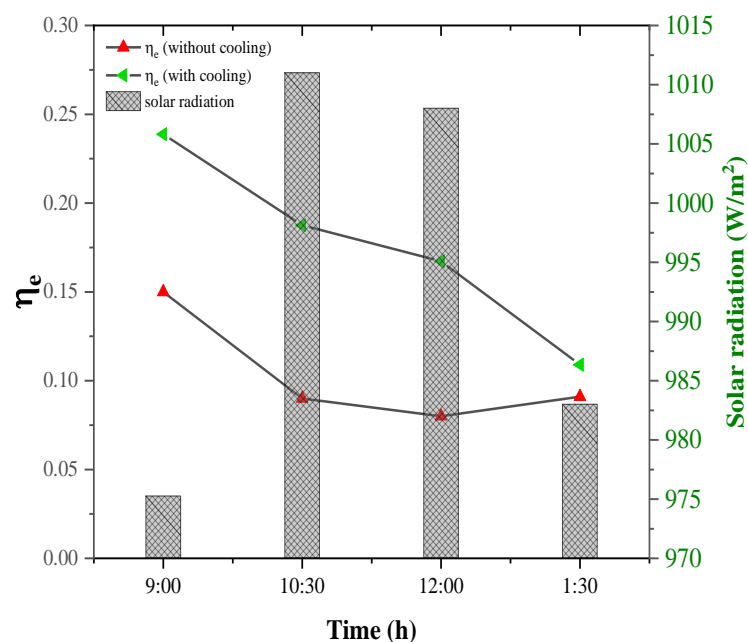

Figure 10. Hourly variations in electrical efficiency for the PVR and PVT modules.

5.3. PVT Thermal, Electrical, and Overall Efficiencies

Figure 11 shows the influence of inlet water temperature and solar radiation on the PVT thermal efficiency. At a constant ambient air velocity and mass flow rate of water at the inlet, the PV thermal efficiency falls as both the inlet water temperature and irradiance levels rise. An increase in irradiance causes a greater temperature gradient between the PVT system and its surroundings because of convective heat transfer. Since more heat is lost at greater irradiance under these conditions, the thermal efficiency drops. Because of this deteriorating trend, heat transfer from PVT material to cooling water is inefficient.
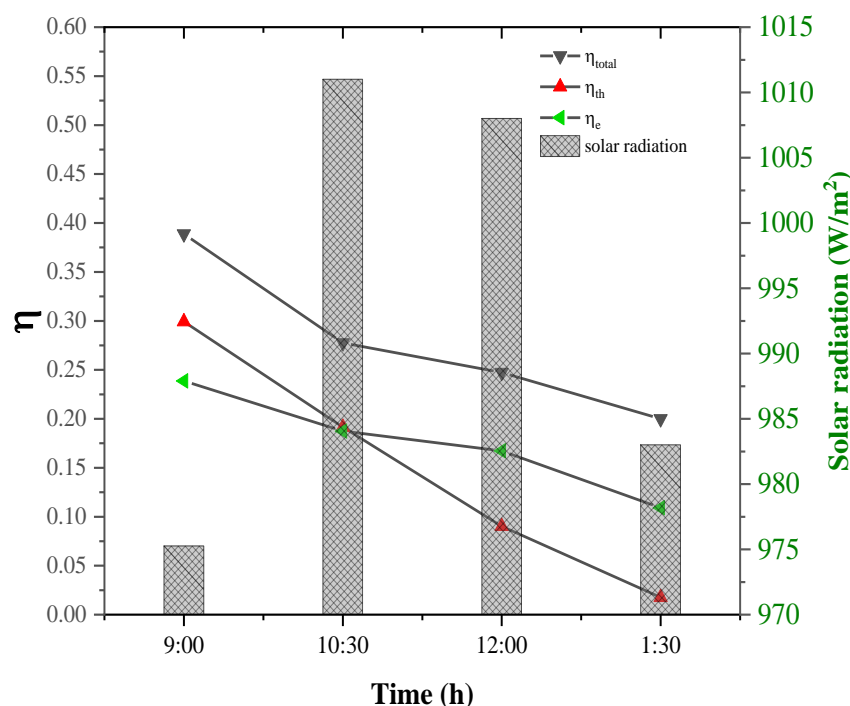

Figure 11. Hourly variation of the PVT total, thermal, and electrical efficiencies.

Consequently, there is a significant drop in efficiency when the irradiance increases and the water temperature at the inlet rises. At 9:00 am, the figure shows the highest thermal efficiency of 30% at 9.00 am. Finally, the lowest efficiency of 2% is found to occur at 1.30 pm. Figure 8 demonstrates the total efficiency of the PVT operating on water drops with rising irradiation levels and inlet water temperature at constant ambient air velocity and water mass flow; as the electrical and irradiance levels increase, thermal efficiency likewise declines. Consequently, as the value of irradiation level changes from 975 to 985 W/m^2, the study reports a decline in overall efficiency, from 39% to 20%. Various operational factors contribute to the PVT system's overall performance, including solar radiation, mass flow rate, ambient temperatures, thermal collector system design, flow pipe diameter, and material.

5.4. Total and Exergy Efficiency

Energy and exergy efficiency for Tehran are computed using Equations (16)–(19) and experimental data from Table 3. Hourly changes in energy and exergy efficiencies are shown in Figure 12. In the figure, total efficiency (20–39%) is greater than exergy efficiency (12–30%). In addition, the highest exergy efficiency (30%) is seen around 9:00 am, while the lowest efficiency (12%). This investigation uses water to transfer heat from the PV surface. However, additional thermal energy may be extracted efficiently and straightforwardly if water is fed below the PV surface in a forced mode. Increased energy and exergy efficiency would result from this. As seen in Figure 10, however, as the water temperatures in the outlet and inlet converge, the thermal energy extracted from the solar cell decreases, resulting in a drop in both total and exergy efficiency.
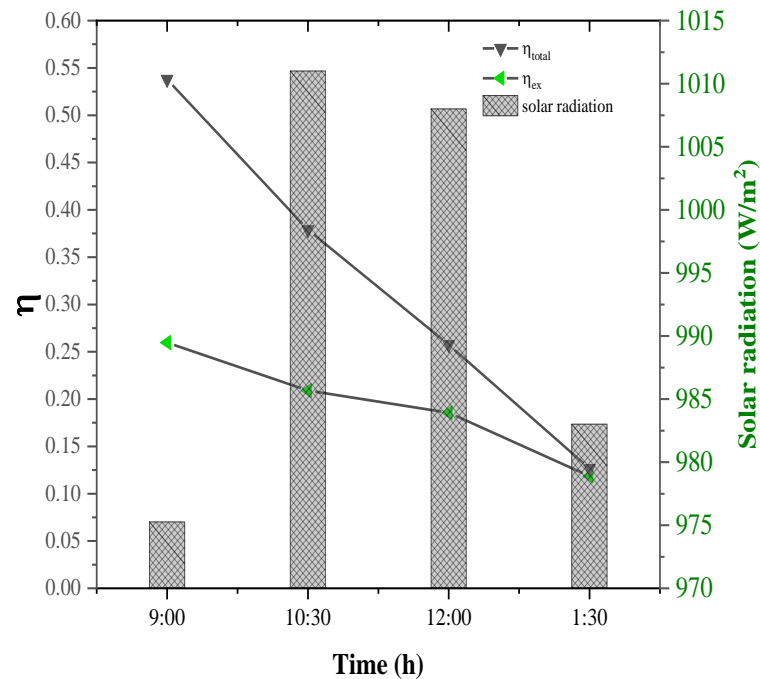
Figure 12. Variations of η_{total} and η_{ex} with different inlet temperatures of the water (T_{amb} = 293.15 K, m = 0.033 kg/s, and V_{wind} = 3 m/s).

5.5. Commercial PVT Systems

Commercial photovoltaic/thermal (PVT) systems are a type of hybrid solar technology that combines photovoltaic panels and solar thermal collectors in a single system. These systems are typically used in commercial or industrial applications, such as large office buildings, factories, or hospitals. Here are some key features and benefits of commercial PVT systems:

1.   High efficiency: PVT systems can achieve higher overall energy efficiency than standalone photovoltaic or solar thermal systems by utilizing the same area of rooftop or land;

2.   Dual function: The dual function of PVT systems means that they can generate both electricity and heat simultaneously, which increases the overall energy output and the overall savings on energy bills;

3.   Reduced space requirements: PVT systems can be used where space is limited or where separate installations of photovoltaic and solar thermal systems would be too expensive;

4.   Improved system lifespan: PVT systems have a longer lifespan than standalone photovoltaic or solar thermal systems since they are able to capture more energy from the sun and therefore experience less thermal stress;

5.   Reduced operating costs: PVT systems can reduce the operating costs of a facility by providing both electricity and heat, reducing the need to purchase electricity from the grid and operate separate heating systems.

Overall, commercial PVT systems offer several benefits, including increased energy efficiency, reduced space requirements, and reduced operating costs. These systems can be an effective solution for commercial or industrial facilities looking to reduce their energy costs and improve their sustainability.

6. Conclusions

The study investigated the effectiveness of a combined photovoltaic thermal module using both experimental and numerical methods. The module incorporates water pipes for cooling, which are connected to the rear of the photovoltaic panel. The study explored the

impact of various variables, including ambient temperature, solar radiation, and fluid inlet temperature, on the efficiency of the module.

The experiments were conducted over four scenarios, with the fluid inlet temperature ranging from 19.5 °C to 61 °C. The application of a cooling water system resulted in a reduction in the PV surface temperature from 58.5 °C to 33.5 °C at 9:00 am and from 71 °C to 68 °C at 1:30 pm. The study found that as the radiation level and the water temperature at the inlet increased, the system's electrical, thermal, overall, and exergy efficiency decreased.

The research employed both experimental and numerical methods, and the results of both methods were compared, and a suitable agreement was found. The study's conclusions provide valuable insights into the efficiency of combined photovoltaic thermal modules and the impact of different variables on their performance.

Nomenclature

$\vec{V}$	Velocity vector
Q	Convective heat transfer (W)
A	Cross-sectional area (m^2)
I	Current (I)
Q	Energy
M	Flow rate (kg/s)
F	Global body force (N)
G	Global irradiance (W/m^2)
H	Heat transfer coefficient (W/m^2 K)
V	Kinematic viscosity (m^2/s)
Mpp	Maximum power point
PV	Photovoltaic
Co	Radiation coefficient
Cp	Specific heat (J/kg, K)
T	Temperature (K)
K	Thermal conductivity (W/m.K)
v	Voltage (V)
V	Wind speed (m/s)
Greek letters	
α	Absorption coefficient
η	Efficiency
ε	Emissivity
ρ	Fluid density (kg/m^3)
τ	Transmissivity coefficient
φ	Viscous dissipation
Subscripts	
amb	Ambient
e	Electric
g	Glass
in	Inlet
o	Open-circuit
out	Outlet
sc	Short circuit
ave	Average
ex	Exergy

References

1. Zhang, X.; Zhao, X.; Smith, S.; Xu, J.; Yu, X. Review of R&D progress and practical application of the solar photovoltaic/thermal (PV/T) technologies. *Renew. Sustain. Energy Rev.* **2012**, *16*, 599–617. [CrossRef]
2. Tao, H.; Alawi, O.A.; Hussein, O.A.; Ahmed, W.; Eltaweel, M.; Homod, R.Z.; Abdelrazek, A.H.; Falah, M.W.; Al-Ansari, N.; Yaseen, Z.M. Influence of water based binary composite nanofluids on thermal performance of solar thermal technologies: Sustainability assessments. *Eng. Appl. Comput. Fluid Mech.* **2023**, *17*. [CrossRef]
3. Meral, M.E.; Dinçer, F. A review of the factors affecting operation and efficiency of photovoltaic based electricity generation systems. *Renew. Sustain. Energy Rev.* **2011**, *15*, 2176–2184. [CrossRef]
4. Dwivedi, P.; Sudhakar, K.; Soni, A.; Solomin, E.; Kirpichnikova, I. Advanced cooling techniques of P.V. modules: A state of art. *Case Stud. Therm. Eng.* **2020**, *21*, 100674. [CrossRef]
5. Verma, S.; Mohapatra, S.; Chowdhury, S.; Dwivedi, G. Cooling techniques of the PV module: A review. *Mater. Today Proc.* **2020**, *38*, 253–258. [CrossRef]
6. Velmurugan, K.; Kumarasamy, S.; Wongwuttanasatian, T.; Seithtanabutara, V. Review of PCM types and suggestions for an applicable cascaded PCM for passive PV module cooling under tropical climate conditions. *J. Clean. Prod.* **2021**, *293*, 126065. [CrossRef]
7. Habib, K.; Ahmed, M.; Abdullah, A.Q.; Alawi, O.A.; Bakthavatchalam, B.; Hussein, O.A. Metallic Oxides for Innovative Refrigerant Thermo-Physical Properties: Mathematical Models. *Tikrit J. Eng. Sci.* **2021**, *29*, 1–15. [CrossRef]
8. Kribus, A.; Kaftori, D.; Mittelman, G.; Hirshfeld, A.; Flitsanov, Y.; Dayan, A. A miniature concentrating photovoltaic and thermal system. *Energy Convers. Manag.* **2006**, *47*, 3582–3590. [CrossRef]
9. Kandilli, C. Performance analysis of a novel concentrating photovoltaic combined system. *Energy Convers. Manag.* **2013**, *67*, 186–196. [CrossRef]
10. Nadda, R.; Kumar, A.; Maithani, R. Efficiency improvement of solar photovoltaic/solar air collectors by using impingement jets: A review. *Renew. Sustain. Energy Rev.* **2018**, *93*, 331–353. [CrossRef]
11. Royne, A.; Dey, C.J.; Mills, D.R. Cooling of photovoltaic cells under concentrated illumination: A critical review. *Sol. Energy Mater. Sol. Cells* **2005**, *86*, 451–483. [CrossRef]
12. Rashid, W.T.; Ahmad, B.A.; Jumaah, A.H. The optimum conditions of Titanium Recovery process from the Iraqi Bauxite Ore. *Tikrit J. Eng. Sci.* **2022**, *29*, 7–14. [CrossRef]
13. Eltaweel, M.; Heggy, A.H.; Yaseen, Z.M.; Alawi, O.A.; Falah, M.W.; Hussein, O.A.; Ahmed, W.; Homod, R.Z.; Abdelrazek, A.H. Application of the ANOVA method in the optimization of a thermoelectric cooler-based dehumidification system. *Energy Rep.* **2022**, *8*, 10533–10545. [CrossRef]
14. Yang, L.; Xuan, Y.; Han, Y.; Tan, J. Investigation on the performance enhancement of silicon solar cells with an assembly grating structure. *Energy Convers. Manag.* **2012**, *54*, 30–37. [CrossRef]
15. Cuce, E.; Cuce, P.M. A comprehensive review on solar cookers. *Appl. Energy* **2013**, *102*, 1399–1421. [CrossRef]
16. Siddiqui, M.U.; Arif, A.; Kelley, L.; Dubowsky, S. Three-dimensional thermal modeling of a photovoltaic module under varying conditions. *Sol. Energy* **2012**, *86*, 2620–2631. [CrossRef]
17. Teo, H.; Lee, P.; Hawlader, M. An active cooling system for photovoltaic modules. *Appl. Energy* **2012**, *90*, 309–315. [CrossRef]
18. Bahaidarah, H.; Subhan, A.; Gandhidasan, P.; Rehman, S. Performance evaluation of a PV (photovoltaic) module by back surface water cooling for hot climatic conditions. *Energy* **2013**, *59*, 445–453. [CrossRef]
19. Bashir, M.; Ali, H.; Amber, K.; Ali, H.; Imran, S.; Kamran, M. Performance investigation of photovoltaic modules by back surface water cooling. *Therm. Sci.* **2018**, *22*, 2401–2411. [CrossRef]
20. Wu, S.-Y.; Chen, C.; Xiao, L. Heat transfer characteristics and performance evaluation of water-cooled PV/T system with cooling channel above PV panel. *Renew. Energy* **2018**, *125*, 936–946. [CrossRef]
21. Shen, C.; Liu, F.; Qiu, S.; Liu, X.; Yao, F.; Zhang, Y. Numerical study on the thermal performance of photovoltaic thermal (PV/T) collector with different parallel cooling channels. *Sustain. Energy Technol. Assess.* **2021**, *45*, 101101. [CrossRef]
22. Nahar, A.; Hasanuzzaman, M.; Rahim, N. Numerical and experimental investigation on the performance of a photovoltaic thermal collector with parallel plate flow channel under different operating conditions in Malaysia. *Sol. Energy* **2017**, *144*, 517–528. [CrossRef]
23. Shen, C.; Zhang, Y.; Zhang, C.; Pu, J.; Wei, S.; Dong, Y. A numerical investigation on optimization of PV/T systems with the field synergy theory. *Appl. Therm. Eng.* **2020**, *185*, 116381. [CrossRef]
24. Salameh, T.; Tawalbeh, M.; Juaidi, A.; Abdallah, R.; Hamid, A.-K. A novel three-dimensional numerical model for PV/T water system in hot climate region. *Renew. Energy* **2020**, *164*, 1320–1333. [CrossRef]
25. Vedulla, G.; Geetha, A.; Senthil, R. Review of Strategies to Mitigate Dust Deposition on Solar Photovoltaic Systems. *Energies* **2022**, *16*, 109. [CrossRef]
26. Coşgun, A.E.; Demir, H. The Experimental Study of Dust Effect on Solar Panel Efficiency. *J. Polytech.* **2021**, *25*, 1429–1434. [CrossRef]
27. Demir, H. Application of Thermal Energy Harvesting from Photovoltaic Panels. *Energies* **2022**, *15*, 8211. [CrossRef]
28. Bhakre, S.S.; Sawarkar, P.D.; Kalamkar, V.R. Performance evaluation of PV panel sfile:///F:/Paper1/PVT-Paper/Ref/2.pdfurfaces exposed to hydraulic cooling—A review. *Sol. Energy* **2020**, *224*, 1193–1209. [CrossRef]

29. Reddy, S.R.; Ebadian, M.A.; Lin, C.-X. A review of PV–T systems: Thermal management and efficiency with single phase cooling. *Int. J. Heat Mass Transf.* **2015**, *91*, 861–871. [CrossRef]

30. Gharzi, M.; Arabhosseini, A.; Gholami, Z.; Rahmati, M.H. Progressive cooling technologies of photovoltaic and concentrated photovoltaic modules: A review of fundamentals, thermal aspects, nanotechnology utilization and enhancing performance. *Sol. Energy* **2020**, *211*, 117–146. [CrossRef]

31. Bhandari, P.; Padalia, D.; Ranakoti, L.; Khargotra, R.; András, K.; Singh, T. Thermo-hydraulic investigation of open micro prism pin fin heat sink having varying prism sides. *Alex. Eng. J.* **2023**, *69*, 457–468. [CrossRef]

32. Swinbank, W.C. Long-wave radiation from clear skies. *Q. J. R. Meteorol. Soc.* **1963**, *89*, 339–348. [CrossRef]

33. Othman, M.; Hamid, S.; Tabook, M.; Sopian, K.; Roslan, M.; Ibarahim, Z. Performance analysis of PV/T Combi with water and air heating system: An experimental study. *Renew. Energy* **2015**, *86*, 716–722. [CrossRef]

34. Wu, S.-Y.; Guo, F.-H.; Xiao, L. A Review on the Methodology for Calculating Heat and Exergy Losses of a Conventional Solar PV/T System. *Int. J. Green Energy* **2014**, *12*, 379–397. [CrossRef]

35. Yang, D.J.; Yuan, Z.F.; Lee, P.H.; Yin, H.M. Simulation and experimental validation of heat transfer in a novel hybrid solar panel. *Int. J. Heat Mass Transf.* **2012**, *55*, 1076–1082. [CrossRef]